Raman spectra of C_{60} dimer and C_{60} polymer confined inside a (10, 10) single-walled carbon nanotube

2010 J. Phys.: Condens. Matter 22 145303

(http://iopscience.iop.org/0953-8984/22/14/145303)

J. Phys.: Condens. Matter **22** (2010) 145303 (9pp) doi:10.1088/0953-8984/22/14/145303

Raman spectra of C_{60} dimer and C_{60} polymer confined inside a (10, 10) single-walled carbon nanotube

H Chadli[1], A Rahmani[1,3] and J-L Sauvajol[2]

[1] Laboratoire de Physique des Matériaux et Modélisation des Systèmes (Unité Associée au CNRST-URAC 08), Université MY Ismaïl, Faculté des Sciences, BP 11201, Zitoune, 50000 Meknès, Morocco
[2] Laboratoire des Colloïdes, Verres et Nanomatériaux (UMR CNRS 5587), Université Montpellier II, 34095 Montpellier Cedex 5, France

Received 19 November 2009, in final form 3 March 2010
Published 25 March 2010
Online at stacks.iop.org/JPhysCM/22/145303

Abstract
A new set of C–C interball force constant was developed in order to reproduce the low wavenumber density of states measured by neutron scattering and the Raman spectra of the C_{60} dimer and C_{60} polymer chain. The nonresonant Raman spectra of the C_{60} dimer and C_{60} polymer confined inside a (10, 10) single-walled carbon nanotube were calculated in the framework of the bond-polarization theory by using the spectral moments method. The main changes of the Raman spectrum as a function of the organization of the C_{60} molecules inside the nanotubes were identified. We found that the radial breathing modes of a (10, 10) single-walled carbon nanotube are more sensitive on the structure of the C_{60} molecules than the G-modes. These predictions are useful to interpret the experimental Raman spectrum of fullerene peapods.

1. Introduction

The new forms of carbon, such as fullerene and single wall carbon nanotube (SWCNT), have attracted considerable interest due to some of their extraordinary properties [1]. A few years ago, it was experimentally shown that fullerenes can be inserted into SWCNTs, forming the so-called peapod-like structure and first electron microscopy images of peapods have revealed the one-dimensional character of the C_{60} chain inside the carbon nanotube [2]. In agreement with calculations [3–5], it was found experimentally that the center-to-center distance between two C_{60} in peapods (0.98 nm) was smaller than in three-dimensional crystals (1.0 nm) but larger than in polymeric fullerenes (typically around 0.95 nm) [6–8]. Theoretically, it was found that the structure of the C_{60} chain inside the nanotube also depends on the diameter of the SWCNT [9–11].

On the other hand, the successful synthesis under high pressure and high temperature treatments (HPHTT) of a solid phase of C_{60} dimer (D), polymerized C_{60} structures including a crystalline one-dimensional orthorhombic (O) phase, and two-dimensional tetragonal (T) and rhombohedral (R) solids has allowed the investigation of phonons of these new compounds by Raman, infrared and neutron spectroscopies [12–16]. Theoretical works [17–19] have investigated the dimerization of C_{60} molecules. It was established that the bonding between two C_{60} molecules occurs by a [2 + 2] cyclo-addition reaction which leads to dimer, trimer ... polymer phases in which C_{60} molecules are bounded by a four membered square ring [20–22]. In recent years, a variety of theoretical methods have been applied to calculate the intra- and interball modes of C_{60} dimer, trimer and polymer chains: *ab initio* calculations [24], tight binding Hamiltonian models [25] and the force constants model [26]. In the last model, introduced by Schober *et al*, the intraball C–C interactions are calculated using a force field proposed by Jishi *et al* [27]. The covalent interball bonds were modeled by a longitudinal and two angular force constants. These force constants were fitted in order to reproduce the experimental low wavenumber (0–200 cm^{-1}) density of states (DOS) derived from inelastic neutron scattering measurements performed on the dimer and polymer phases of RbC_{60} [26]. In the present work, modifications of the Schober force constants will be done in order to fit both the density of states and Raman-active modes of C_{60} dimer and polymer phases.

Raman spectroscopy has been demonstrated to be a key technique to characterize carbon-based nanostructures.

[3] Author to whom any correspondence should be addressed.

Group theory analysis applied to the C_{60} molecule shows that the totally symmetric irreducible representation A_g (non-degenerate first-order Raman-active modes) is realized twice, H_g (five-fold degenerate first-order Raman-active modes) occurs eight times, and T_{1u} (zero frequency mode and four three-fold degenerate infrared-active modes) occurs five times. A first Raman experiment on peapods has been performed at helium temperature to avoid a possible photopolymerization of C_{60} molecules under laser irradiation [28]. A Raman-active mode located at 90 cm^{-1}, close to the interball C_{60} dimer mode, was observed. As follows, Pfeiffer *et al* [29] have performed a detailed Raman investigation on peapods organized in bundles, and focused on the dependence of the C_{60} modes with temperature and excitation energy. The temperature dependencies of the Ag(1) and Ag(2) modes of C_{60} have been measured at different excitation energies. At 90 K, both the Ag(1) mode, around 497 cm^{-1} in C_{60}, and the Ag(2) mode, around 1469 cm^{-1} in C_{60}, are split in two components, downshifted and upshifted with respect to the position of the corresponding modes in the crystalline phase of C_{60}. The splitting of the Ag(2) mode is rather surprising and it was understood as the spectroscopic fingerprint of the different mobilities of C_{60} molecules inside the nanotubes [29].

In our first work, [30], and its complete version [11] focused on C_{60} monomer peapods (with linear and zigzag phases) only, we have studied the different possible configurations of C_{60} monomers inside single wall carbon nanotubes and found that the C_{60} molecules adopt a linear configuration for diameters below 1.45 nm and a zigzag configuration for diameters between 1.45 and 2.20 nm. The nonresonant Raman spectra of these phases have been calculated. Our results are in part in qualitative agreement with the experimental ones. In particular, a splitting of the Ag(1) mode of C_{60} was predicted by calculations. By contrast, no splitting of the Ag(2) mode was calculated, suggesting that the experimental splitting could be the signature of the presence of C_{60} oligomers inside the nanotube. Concerning the modes of SWCNTs encasing C_{60} molecules, it has been reported experimentally that [31, 32]: (i) for SWCNTs in the diameter range 1.45–1.76 nm, the radial breathing-like mode (RBLM) was downshifted compared to the RBM of empty SWCNTs, and (ii) for smaller diameters, two RBLM components, upshifted and downshifted with regards to the position of the RBM of the empty tube, were measured. We have suggested that the presence of two radial breathing-like modes could be related either to a low C_{60} filling factor or to the presence of zigzag C_{60} chains inside the nanotubes [11].

In this paper, in order to complete our study about the vibrations of C_{60} molecules confined inside carbon nanotubes, we investigate the effect of dimerization and polymerization of C_{60} molecules on the Raman spectra of C_{60} peapods. Indeed, C_{60}s covalently bonded with [2 + 2] cyclo-addition was identified in peapod samples. We report the structure and the force constants model of the isolated C_{60} polymer chain. The C–C intraball force constants were fitted in order to obtain a good description of the phonon in the C_{60} dimer and polymer measured by inelastic neutron scattering and Raman spectroscopy. This approach is very fast and gives a good fit to experimental vibrational spectra. Depending on the nanotube diameter, different configurations of dimerized and polymerized C_{60} molecules confined inside SWCNT can certainly exist [11]. However, since the synthesized peapod diameters are around a (10, 10) nanotube, we restrict our study by considering only a typical linear chain of C_{60} dimers and a C_{60} polymer chain confined inside a (10, 10) SWCNT. In order to improve the comparison between the calculations and experimental data, linear and zigzag chains of C_{60} dimer and polymer inside carbon nanotubes with different diameters are under study. After a brief description of the force constants and computational model (section 2), the Raman spectra of C_{60} dimer and C_{60} polymer chains either free or confined inside a (10, 10) SWCNT are reported and discussed (section 3).

2. Models and methods

2.1. Structure and dynamics of C_{60} dimer and C_{60} polymer chains

The geometry of the C_{60} dimer molecule can be obtained by joining two C_{60} molecules by parallel double bonds. Other orientations and relative connections between molecules would be possible in principle, but previous calculations have shown that they are energetically unfavorable with respect to [2 + 2] cyclo-addition [17, 24, 34]. The geometry optimization of the [2 + 2] dimerized C_{60} molecule was performed using a molecular mechanics method (MM2 force) [33]. The optimized structures of the C_{60} dimer, trimer and infinite polymer chains are shown in figure 1. We found that the length between the carbon atoms participating in the [2 + 2] cyclo-addition change: the intrafullerene bond lengths shift from 0.139 to 0.15 nm for double bonds and from 0.142 to 0.153 nm for single bonds. On the other hand, the length of the interfullerene bonds are close to 0.153 nm. The formation of intermolecular bonds reduces the symmetry of individual C_{60} from I_h to D_{2h}.

To calculate the phonon modes of the C_{60} dimer and C_{60} polymer, Schober *et al* [26] used the force constants of Jishi [27], which well describe the C–C interactions in C_{60} (intraball). In this model, each atom is assumed to be a point mass, and to be connected with springs to its first-, second-, and third-nearest neighbors. Two springs, with spring constants s_p and s_h, are used to model the stretching of the pentagonal and hexagonal covalent bonds, respectively. The force constants of the springs connecting an atom to its second- and third-nearest neighbor are denoted by s_2 and s_3, respectively. The bending of the pentagonal and hexagonal angles are modeled by springs with spring constants a_p and a_h, respectively. In addition, the bending of the angles between the spring connecting an atom to its first-nearest neighbor and the spring connecting it to its second- and third-nearest neighbors are modeled by spring constants b and c, respectively. The potential energy of the molecule is the sum of the stretching and bending contributions.

Let us for example, consider three atoms labeled i, j, and k, where j is a second-nearest neighbor of i. Upon giving arbitrary displacements to these three atoms, the

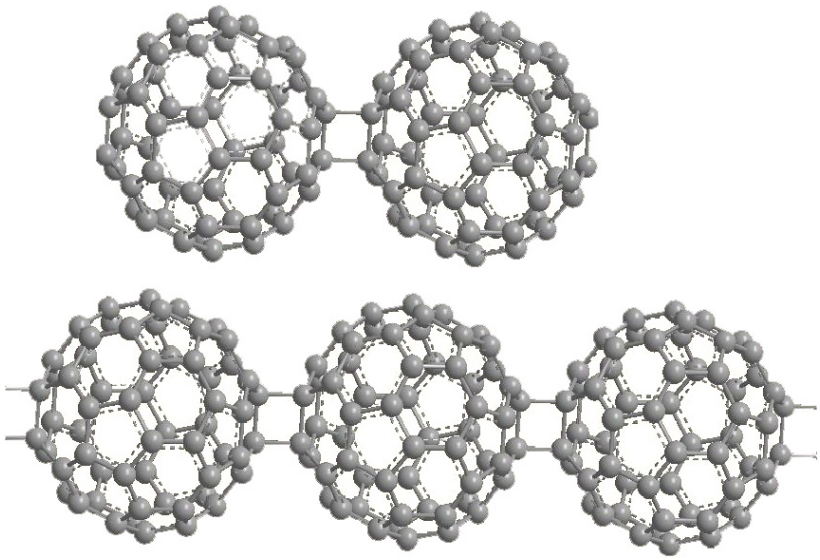

Figure 1. Geometries for two structures of C_{60}: the dimer and infinite polymer chain.

Table 1. Force constant parameters for intrafullerene bonds (D0 model). D1 and P models represent interfullerene dimer and polymer force constants respectively. The bond-stretching force constants are expressed in (mdyn $Å^{-1}$), whereas the angle-bending force are expressed in (mdyn rad^{-2}).

Model	Stretching	Value	Bending	Value
D_0	s_p	3.95	a_p	1.0
	s_h	2.30	b_h	0.25
	s_2	1.21	b	0.095
	s_3	−1.05	c	0.235
			K_1	0.36
D	K_{str}	2.1	K_2	0.34
			K_1	0.8
P	K_{str}	4.0	K_2	0.7

contribution to the potential energy of the stretching of the spring connecting i to k is given by

$$\boldsymbol{V}_s^{ik} = \tfrac{1}{2}s_2(\triangle r_{ik})^2, \tag{1}$$

where $\triangle r_{ik}$ is the change in distance between atoms i and k. On the other hand, the contribution to the potential energy due to the bending of the angle $(\boldsymbol{ij}, \boldsymbol{ik})$ is given by

$$\boldsymbol{V}_b(\boldsymbol{ij}, \boldsymbol{ik}) = \tfrac{1}{2}b(\triangle\theta)^2, \tag{2}$$

$\triangle\theta$ is the change in the angle $(\boldsymbol{ij}, \boldsymbol{ik})$ due to the displacements given to atoms i, j and k.

The values of the bond-stretching and angle-bending force constants used to obtain the best fit to the experimental Raman data are given in table 1.

Concerning the interball bonds, they were modeled by a stretching force constant K_{str} for the interball C–C bond and two angle-bending force constants: K_1 is related to the angle spanned by interball C–C bond and the (6, 6) bond, K_2 to the angles spanned by the interball C–C bond and the (5, 6) bond. These three parameters were fitted to optimize the description of the low wavenumber part of the vibrational-density-of-states (DOS) measured by neutron scattering in RbC_{60} dimer and RbC_{60} polymeric phases. These force constants (D_1 and P_1 for dimer and polymer respectively) are given in table 2 of [26].

It was experimentally found that the Ag(2) mode shifts from 1469 cm^{-1} in the pristine solid phase of C_{60} to 1459 cm^{-1} in the photopolymerized state [45]. Using the force constants of Schober and in order to reproduce the low wavenumber region of the DOS and Raman spectra of the C_{60} dimer and C_{60} polymer, a modification of the force constants describing the C–C intraball interactions (D_0 model) as well as the C–C interball interactions (D model for the dimer and the P model for the polymer) has been performed. Our adjusted force constants are given in table 1. We use the same units as the Born–von Karman force constants of Jishi for the bond-stretching (mdyn $Å^{-1}$), and the angle-bending force (mdyn rad^{-2}).

2.2. Structure and dynamics of C_{60} peapods

A carbon peapod consists of C_{60} molecules trapped inside a single wall carbon nanotube host. In this study, we consider peapods in which the encapsulated C_{60} molecules are covalently bonded by [2 + 2] cyclo-addition reaction. The SWCNT C–C intratube interactions are described using a force constant model introduced by Saito *et al* [35]. Previously, we used the same model to calculate the nonresonant Raman spectra of single wall carbon nanotubes of different lengths [36].

The C–C interaction between carbon atoms belonging to non-bonded fullerenes, and between fullerenes and the surrounding nanotube, are represented by the Lennard-Jones potential, $U_{LJ} = 4\epsilon[(\sigma/R)^{12} - (\sigma/R)^6]$. The values of the Lennard-Jones parameters were chosen as $\epsilon = 2.964$ meV and $\sigma = 0.3407$ nm. These values have recently been found to describe correctly the van der Waals contribution to the C_{60} bulk cohesive energy [37]. To derive the elements of the dynamical matrix, we used a van der Waals cut-off radius of 0.74 nm.

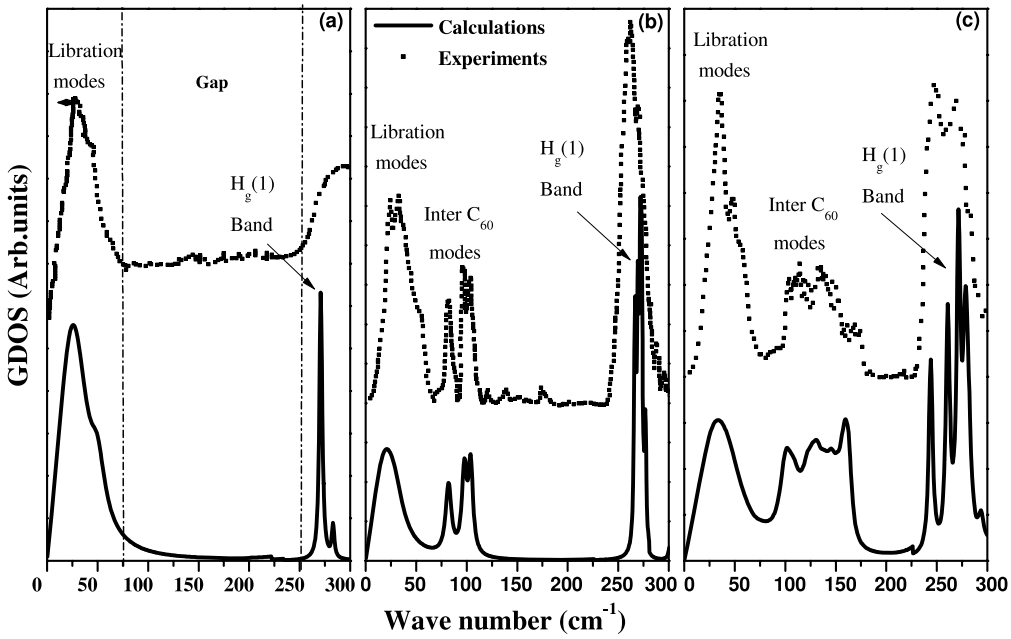

Figure 2. Comparison between lattice dynamical calculations and the experimental [42] density of states for C_{60} monomer (curve a), dimer (curve b) and infinite 1D polymer (curve c).

The optimal dimer–dimer gap was calculated by minimization of the Lennard-Jones inter-dimers and dimer–nanotube interactions. In order to obtain the optimal configuration of the C_{60} dimer and polymer inside the nanotubes, an energy minimization was performed using the same procedure described in our previous calculations [11]. We found that the nearest separation between the inserted C_{60} oligomers (dimer, polymer) and the nanotube wall is around van der Waals distance (∼0.3 nm) whereas the van der Waals interball separation between two adjacent C_{60} oligomers is around 1.0 nm. This value is in good agreement with the 0.97 nm interball separation measured by electron diffraction [38] and 0.95 nm from high-resolution transmission electron microscopy (TEM) data [39]. Calculations of the Raman spectra, before and after energy minimization, with respect to the relative Euler angles describing the orientation of C_{60} molecules, do not show significant difference in the mode frequencies.

2.3. Methods

The intensities of the Raman lines were calculated within the empirical nonresonant bond polarizability model [40]. Raman spectra are calculated using direct diagonalization of the dynamical matrix for small samples (few hundreds atoms) and the spectral moments method (SMM) [36, 41] for larger ones. For small samples, and as expected, both approaches lead exactly to the same position and intensity for the different modes.

3. Results and discussion

In this section, we are first interested in the vibrational density of states (VDOS) and Raman spectra of the free C_{60} dimer and C_{60} polymer. In the following, we report the results of the calculated Raman spectra for an isolated SWCNT filled with a chain of C_{60} dimers and a C_{60} polymer chain. In all our calculations, we consider the Z direction as the nanotube axis direction and the direction of elongation of the C_{60} dimer and C_{60} polymer chain. We mainly discuss the polarized ZZ Raman spectra for which the polarization direction of the incident and scattered light are along the Z direction.

3.1. Density of states of C_{60} dimer and C_{60} polymer chains

The profile of the density of states (DOS) calculated by using our new set of force constant values is displayed in figure 2 in the low wavenumber range (0–300 cm^{-1}). The comparison with the experimental DOS [42, 26] shows that the main vibration bands are well reproduced by our model. Upon dimerization and polymerization of C_{60} molecules, one of the most significant change of the density of states is the appearance in the low wavenumber range of new modes which were assigned to the intramolecular mixing of the zero-energy translational and rotational modes of individual balls. No such vibrational mode is measured and calculated in the 50–200 cm^{-1} wavenumber range for a chain formed by C_{60} monomers bonded by van der Waals interactions [27]. In dimer and polymer DOS spectra, the latter region is characterized by libration around axes perpendicular to the chain direction produced by the four-fold ring distortion and translation due to the C_{60} displacements along the chain direction. The broadening of the $H_g(1)$ band is related to the splitting of this mode due to dimerization and polymerization. The observed discrepancies between theory and experiments around the Hg mode at 275 cm^{-1} could be associated to the presence of different fullerene structures in the investigated samples in comparison with calculations for the isolated C_{60} monomer

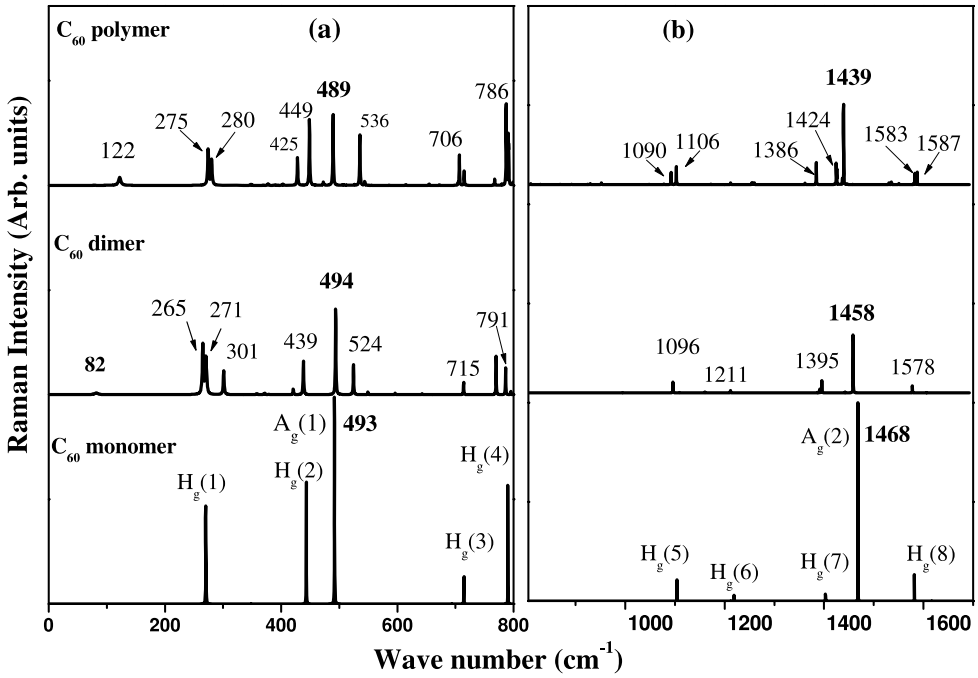

Figure 3. The calculated polarized ZZ Raman spectra of C_{60} monomer, C_{60} dimer, and infinite C_{60} polymer chains. Spectra are displayed in the low (left) and high (right) frequency regions.

(figure 2(a)). In addition, the resolution of the neutron experiment decreases with the energy transfer. In consequence, an experimental broadening of the high frequency peaks is expected. The experimental data are in relatively good agreement with the sum of the broadened calculated peaks. The significant difference in the line shape of the dimer and polymer between 100 and 200 cm^{-1}, which is well reproduced by our calculations, is a good test to validate our approach. The very low wavenumber region is dominated by a band (around 25 cm^{-1}) attributed to a torsion mode where the balls are twisted around the chain axis. The shortness of the expected peak, assigned to the C_{60} libration and located around 25 cm^{-1}, when compared to experimental data (figure 2(c)), could be understood in terms of environment effects: the presence of different polymeric phases where each ball is bound to two (one-dimensional orthorhombic phase), four (two-dimensional tetragonal phase) and six (rhombohedral phase) neighbors in the studied samples. Librations are expected to be more dependent of the environment than intra-C_{60} modes.

3.2. Raman-active modes of C_{60} dimer and C_{60} polymer chains

Using our modified bond force constants together with the bond-charge polarizability parameters of Snoke and Cardona [44], we have investigated the Raman-active modes of C_{60} dimer and polymer chains. The calculated polarized ZZ Raman spectra for the C_{60} dimer and C_{60} polymer are shown in figure 3. Calculated spectra are displayed in the 0–800 cm^{-1} (figure 3(a)) and 800–1600 cm^{-1} (figure 3(b)) ranges respectively. From C_{60} spectra, one recognizes the eight $H_g(1), \ldots, H_g(8)$ and the two $A_g(1)$ and $A_g(2)$ Raman-active modes of the C_{60} monomer. In table 2, we present measured and calculated frequencies for the Raman-active modes of C_{60} in comparison with the results in [23]. We note that our calculated frequencies of the Raman-active modes agree well with the experimental data of [49].

Table 2. Measured and calculated frequencies (in cm^{-1}) for the Raman-active modes C_{60}.

Experimental	Assignment	This work/Ref. [23]
491	$A_g(1)$	493/537
1468	$A_g(2)$	1468/1680
265	$H_g(1)$	270/249
434	$H_g(2)$	443/413
711	$H_g(3)$	715/681
773	$H_g(4)$	790/845
1100	$H_g(5)$	1104/1209
1255	$H_g(6)$	1219/1453
1427	$H_g(7)$	1423/1624
1575	$H_g(8)$	1582/1726

The C_{60} dimer and polymer belong to the D_{2h} point group and all of the first-order Raman-active modes belong to the even-parity irreducible representations A_g, B_{1g}, B_{2g} and B_{3g}. In the 200–600 and 1400–1600 cm^{-1} ranges, the new resolved features in the dimer and polymer spectra are assigned to modes derived primarily from A_g and H_g parent symmetries. As noted above, our calculations (figures 3 and 4) concern the ZZ polarized spectra (Z direction parallel to chain direction) and in accordance with polarizability tensor components (zz component equal to zero for B symmetry in D_{2h} group), all the Raman lines are full-symmetric A_g modes.

Concerning the low wavenumber modes range, below 200 cm^{-1}, no mode is expected in free C_{60} (figure 3(a), bottom). By contrast, in the C_{60} dimer, three interball modes

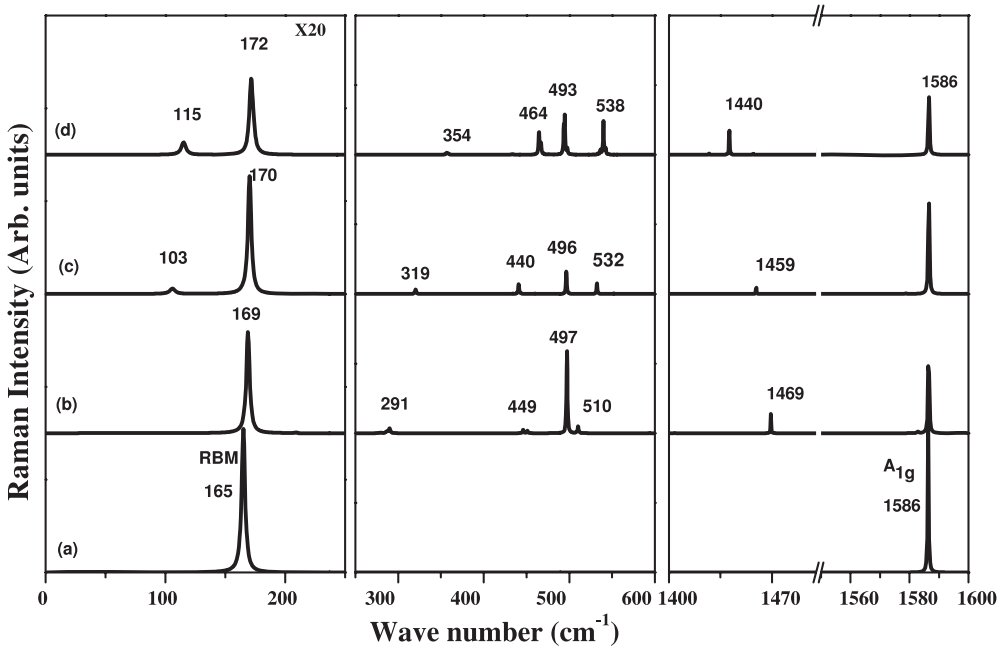

Figure 4. The calculated ZZ polarized Raman spectra of infinite peapods: $(C_{60})_1$@(10, 10) (curve b), $(C_{60})_2$@(10, 10) (curve c) and $(C_{60})_\infty$@(10, 10) (curve d). The calculated Raman spectrum of the empty SWCNT is displayed (curve a).

are calculated at 106, 99, and 82 cm^{-1} (123, 111 and 69 cm^{-1} and figure 8 patterns in [24]). The most Raman active of the three modes is the one at 82 cm^{-1} (figure 3(a), middle). Since this vibrational mode is the lowest wavenumber mode of the A_g representation, one can attribute this mode to the one observed approximately at 96 cm^{-1} [43] for a C_{60} dimer. This same mode is calculated at 69 cm^{-1} and 89 cm^{-1} by *ab initio* [24] and density-functional-based nonorthogonal tight-bending (DF-TB) approaches [46] respectively. The calculated pattern for this mode shows that it is the analog of the stretching mode in a diatomic molecule (figure 8(a)) in [24]. The Raman spectrum of the C_{60} polymer chain features five peaks at 77, 88, 100, 122 and 135 cm^{-1}. The most Raman active is the one at 122 cm^{-1} (figure 3(a), top). The calculated patterns of these Raman-active modes obtained in this work are analogous to that reported in [24] (figure 9). Experimentally, the Raman spectrum of photopolymerized C_{60} shows a new Raman-active mode at 118 cm^{-1} [45, 48], which is in a good agreement with the Raman-active mode calculated at 122 cm^{-1} for a C_{60} polymer chain.

The $H_g(1)$ mode, calculated at 270 cm^{-1} in C_{60} (figure 3(a) bottom), splits in the C_{60} dimer (figure 3(a) middle) and C_{60} polymer (figure 3(a), top). Three modes at 265, 272 and 301 cm^{-1} in the C_{60} dimer and four modes at 242, 270, 280 and 348 cm^{-1} in the C_{60} polymer are calculated. Experiments [45] show a peak at 270 cm^{-1} for pure C_{60}, and peaks at 259, 271 and 300 cm^{-1} for the photopolymerized material, in qualitative agreement with our predictions.

No shift of the $A_g(1)$ mode, located at 493 cm^{-1} in C_{60}, was measured experimentally in the C_{60} dimer and C_{60} polymer. In agreement with experiment, no shift of the $A_g(1)$ mode is calculated in the C_{60} dimer (494.0 ± 1.7 cm^{-1}). By contrast, a downshift of about 5 cm^{-1} is predicted in the C_{60} polymer. This latter behavior has been reported by others using first-principles density-functional techniques [24] and it can be related to the coupling between different modes, in this region, for the C_{60} polymer. In the dimer spectrum, the five-fold degenerate $H_g(2)$ mode, located at 443 cm^{-1} in C_{60}, splits and causes new peaks (located at 421, 439, 524 and 548 cm^{-1}) in the vicinity of the $A_g(1)$ mode (figure 3). The same behavior is obtained in the C_{60} polymer with new peaks around the $A_g(1)$ (489 cm^{-1}): 427, 449, 473, 535, 543 cm^{-1}. Let us note that the $H_g(3)$ mode located at 715 cm^{-1} is not affected by dimerization but splits after polymerization (706, 715 cm^{-1}). After dimerization and polymerization, in the vicinity of the $H_g(4)$ mode located at 790 cm^{-1} in C_{60}, the Raman spectra show new peaks (770, 787 and 795 cm^{-1} for the dimer and 768, 780, 788, 791, 801 and 810 cm^{-1} for the polymer). These new peaks can be attributed to a C_{60} deformation induced by [2 + 2] bonding in dimer and polymer structures.

In figure 3(b), we compare the 800–1600 cm^{-1} region of the calculated Raman spectra of C_{60} monomer, C_{60} dimer, and C_{60} polymer chains. Of particular interest is the calculated shift of the Ag(2) mode. As shown in figure 3(b), this mode shifts from 1468 cm^{-1} in C_{60} (figure 3(b), bottom) to 1458 cm^{-1} in the C_{60} dimer (figure 3(b), middle) and to 1439 cm^{-1} in the C_{60} polymer chain (figure 3(b), top). The values of the shifts are close to those found by *ab initio* calculations [24]. The calculated 10 cm^{-1} shift from the C_{60} monomer to C_{60} dimer agrees well with the observed shift of 10 cm^{-1} from the pristine C_{60} solid phase to the C_{60} photopolymerized state [45, 47]. These shifts are mainly related to the local geometry changes of the individual balls rather than by vibrations coming from the interball interactions. The calculated five-fold degenerate modes, in the high wavenumber range, downshift after dimerization (from 1104 to 1096, 1219

to 1211, 1403 to 1395 and 1582 to 1578 cm^{-1} for $H_g(5)$, $H_g(6)$, $H_g(7)$ and $H_g(8)$, respectively) and split after polymerization. Experimentally, a downshift of about 6 cm^{-1} was measured for the $H_g(8)$ mode [45], which is in agreement with the calculated effect obtained for the $H_g(8)$ dimer mode (from 1582 to 1578 cm^{-1}: 4.0 ± 1.7 cm^{-1}).

3.3. Raman spectra of a linear chain of C_{60} dimers and a linear polymerized chain of C_{60} encapsulated inside a (10, 10) SWCNT

Based on the agreement between experiment and calculations for the C_{60} dimer and C_{60} polymer, we use the same set of force constants to calculate the Raman spectrum of a linear chain of C_{60} dimers and a C_{60} polymer chain encapsulated inside a SWCNT.

Recently we have studied the different possible configurations of C_{60} monomers inside single wall carbon nanotubes and found that the C_{60} molecules adopt a linear configuration for diameters below 1.45 nm and a zigzag configuration for diameters between 1.45 and 2.20 nm [11]. Depending on the nanotube diameter, different configurations of dimerized and polymerized C_{60} molecules confined inside SWCNT can certainly exist. However, in this work we restrict our study by considering only a linear chain of C_{60} dimers and a C_{60} polymer chain confined inside a (10, 10) SWCNT. Indeed, because the diameter of (10, 10) SWCNT fits the diameter of a C_{60} molecule, a linear chain is the most probable configuration [11]. Finally, we deal with completely filled nanotubes.

In figure 4 are compared the polarized ZZ Raman spectrum of (10, 10) SWCNT with those of three kinds of nanopeapods: (i) a linear chain of C_{60} monomers confined into a (10, 10) SWCNT and called in the following as $(C_{60})_1$@(10, 10), (ii) a linear chain of C_{60} dimers confined into a (10, 10) SWCNT (as $(C_{60})_2$@(10, 10)), and (iii) a linear polymer chain of C_{60} molecules confined into a (10, 10) SWCNT (as $(C_{60})_\infty$@(10, 10)).

The well-known radial breathing mode (RBM) of a (10, 10) SWCNT, located at 165 cm^{-1}, exhibits an upshift when the nanotube is filled (figure 4 left): it is located at 169 cm^{-1} in $(C_{60})_1$@(10, 10), at 170 cm^{-1} in $(C_{60})_2$@(10, 10) and 172 cm^{-1} in $(C_{60})_\infty$@(10, 10). We note that the interball–tube interactions affect the RBM mode patterns and the eigenvector of this mode shows an hexagonal SWCNT deformation. By contrast, the position of the high frequency G-mode slightly depends on the filling of the nanotube. It is located at 1586 cm^{-1} either in (10, 10) SWCNT or in the three nanopeapods (figure 4 right).

More significant are the changes of the modes of C_{60} molecules when they are confined inside a (10, 10) SWCNT. In the low wavenumber range, the interball mode located at 82 cm^{-1} for a free C_{60} dimer (figure 3 middle) is upshifted to 103 cm^{-1} in $(C_{60})_2$@(10, 10) (figure 4 left). By contrast, the intraball mode located at 122 cm^{-1} for a free polymeric chain of C_{60} molecules (figure 3 top) is downshifted to 115 cm^{-1} in $(C_{60})_\infty$@ (10, 10) SWCNT (figure 4 left). The frequency and the vibration pattern of these modes are determined by the competitions between the ball–nanotube and intraball interactions.

As we have mentioned before, the single Hg(1) mode, located at 270 cm^{-1} in the C_{60} monomer, splits into three and four components in the C_{60} dimer and C_{60} polymer respectively (figure 3). As these different C_{60} structures are confined inside the (10, 10) nanotube, all these components split and shift, leading to the observation of a multipeak band dominated by a mode located around 291, 319 and 354 cm^{-1} in monomer, dimer and polymer peapods, respectively. This behavior is due to the lower symmetry of the environment introduced by polymerization and the chain–nanotube interaction effects.

In the range of the $A_g(1)$ mode (figure 3, bottom), three main components are calculated at: (449, 497, 510), (440, 496, 532) and (464, 493, 538) cm^{-1} for $(C_{60})_1$@(10, 10), $(C_{60})_2$@(10, 10) and $(C_{60})_\infty$@(10, 10), respectively. The position of the highest component, non-Raman active in free C_{60} (figure 3 bottom), is upshifted by about to 12 (28) cm^{-1} from the monomer to dimer (polymer) peapods. The lowest component located around the $H_g(2)$ mode ($\sim$443 cm^{-1} in free C_{60}) downshifts (upshifts) by about 9 (15) cm^{-1} from the monomer to dimer (polymer) peapods. As for isolated chains, the $A_g(1)$ mode frequency is not affected after dimerization, and a downshift of about 4 cm^{-1} is calculated in the polymerized peapod. The calculated shifts from the isolated to encapsulated chains arise from the dispersion introduced in modes by the van der Waals C_{60}–nanotube interactions.

Finally, concerning the high wavenumber range, we show that the $A_g(2)$ mode of the free C_{60}, C_{60} dimer and C_{60} polymer is not affected (an upshift of about 1 cm^{-1}) when they are confined into a (10, 10) SWCNT. They are located at 1469 cm^{-1}, 1459 cm^{-1} and 1440 cm^{-1} in $(C_{60})_1$@(10, 10), $(C_{60})_2$@(10, 10) and $(C_{60})_\infty$@(10, 10), respectively.

These predictions can be compared with the experimental data available on peapods. Raman spectra of C_{60} molecules confined into SWCNTs having diameters between 1.36 and of 1.47 nm have been reported in [28]. For the investigated samples, comparison between experiment and calculation suggest the presence of C_{60} oligomers confined inside the nanotubes. The measured Raman spectra show a mode around 90 cm^{-1}. From our calculations, this mode can be assigned to the stretching mode between bonded fullerenes in the C_{60} dimer or C_{60} polymer confined inside the SWCNT. No such mode is predicted in $(C_{60})_1$@(10, 10). Calculations predict a significant downshift of the free C_{60} Ag(2) mode either in the free or confined C_{60} dimers and C_{60} polymer. From figure 5(a) in [28], the Raman spectrum of the studied sample is dominated by a large band centered around 1467 cm^{-1}, which is close to the position of the Ag(2) mode in free C_{60}. Additionally, one can observe weak Raman-active mode intensities in the range of the predicted Ag(2) mode for the C_{60} dimer (1459 cm^{-1}) and C_{60} polymer (1440 cm^{-1}). These Ag(2) mode intensity ratios can be understood in terms of symmetry considerations in individual C_{60} in comparison with C_{60} oligomers. Our calculations within the nonresonant polarizability model confirm this intensity behavior qualitatively.

On the other hand, Pfeiffer *et al* have performed a detailed Raman investigation on peapods organized in bundles [29].

The mean diameter of the SWCNTs are 1.31, 1.34 and 1.40 nm, which are consistent with the presence of linear peapods [11]. These authors found two components in the Ag(2) mode range of C_{60}. These components are downshifted (1466 cm^{-1}) and upshifted (1472 cm^{-1}) with respect to the position of the Ag(2) mode in C_{60} (1469 cm^{-1}). Such a splitting of the Ag(2) mode is not predicted as well in the present work as in previous studies [11]. From this study, a downshift of the Ag(2) mode can be produced by a C_{60} polymerization whereas an upshift could be a consequence of the confinement of C_{60} oligomer inside SWCNT. So, the mode at 1466 cm^{-1} could be assigned as the signature of C_{60} oligomers in the sample under consideration. The analysis of the measured Raman spectra, in the low wavenumber range (not available), is required to confirm this suggestion. The new mode at 1472 cm^{-1}, which exhibits a slight upshift with respect to its position in C_{60}, could be assigned as the signature of the presence of unbounded C_{60} inside the nanotube. Consequently, the peapod sample used in the Pfeiffer *et al* experiments could be viewed as a mixing of C_{60} oligomers and C_{60} molecules confined into the nanotube.

4. Conclusion

In this paper, vibrations in the C_{60} dimer and C_{60} polymer, either free or confined inside SWCNTs, have been reported and discussed. A new set of C–C interball force constants have been adjusted in order to reproduce the low wavenumber density of states measured by neutron scattering and the Raman spectra of C_{60} dimer and C_{60} polymer chains. Using these force constants, the polarized nonresonant Raman spectra of linear chains of C_{60} monomers, C_{60} dimers and C_{60} polymers confined inside a (10, 10) SWCNT were calculated. Shifts of the modes of C_{60} and those of SWCNT were predicted under encapsulation. The most significant changes of the Raman spectrum occur in the low wavenumber range, where the inter-C_{60} modes and radial breathing mode of SWCNT are Raman active. These predictions are compared with experimental results suggesting that the Raman spectra of peapods reported in literature are sample dependent and the C_{60} oligomer seems to be present in the majority of the samples investigated.

Acknowledgments

The work was supported by the CNRS-France/CNRST-Morocco agreement.

References

[1] Dresselhaus M S, Dresselhaus G and Eklund P C 1996 *Science of Fullerenes and Carbon Nanotubes* (San Diego, CA: Academic)
[2] Smith B W, Monthioux M and Luzzi D 1998 *Nature* **396** 323
[3] Okada S, Saito S and Oshiyama A 2001 *Phys. Rev. Lett.* **86** 3835
[4] Okada S, Otani M and Oshiyama A 2003 *Phys. Rev.* B **67** 205411
[5] Rochfort A 2003 *Phys. Rev.* B **67** 115401
[6] Smith B W, Russo R M, Chikkannanavar S B and Luzzi D E 2002 *J. Appl. Phys.* **91** 9333
[7] Hirahara K, Suenaga K, Bandow S, Kato H, Okazaki T, Shinohara H and Iijima S 2000 *Phys. Rev. Lett.* **85** 5384
[8] Hirahara K, Bandow S, Suenaga K, Kato H, Okazaki T, Shinohara H and Iijima S 2001 *Phys. Rev.* B **64** 115420
[9] Hodak M and Girifalco L A 2003 *Phys. Rev.* B **68** 085405
[10] Michel K H, Verberck B and Nikolaev A V 2005 *Phys. Rev. Lett.* **95** 185506
[11] Chadli H, Rahmani A, Sbai K, Hermet P, Rols S and Sauvajol J L 2006 *Phys. Rev.* B **74** 205412
[12] Sloan J, Dunin-Borkowski R E, Hutchison J L, Coleman K S, Clifford Williams V, Claridge J B, York A P E, Xu C, Bailey S R, Brown G, Friedrichs S and Green M L H 2000 *Chem. Phys. Lett.* **316** 191
[13] Smith B W, Monthioux M and Luzzi D E 1999 *Chem. Phys. Lett.* **315** 31
[14] Kamarás K, Iwasa Y and Forró L 1999 *Phys. Rev.* B **55** 10999
[15] Davydov V A, Kashevarova L S, Rakhmanina A V, Senyavin V M, Céolin R, Szwarc H, Allouchi H and Agafonov V 2000 *Phys. Rev.* B **61** 11936
[16] Rols S, Cambedouzou J, Bantignies J-L, Rachdi F, Sauvajol J-L, Agafonov V, Rakhmanina A V, Davydov V A, Hennion B and Kahn R 2004 *Phys. Rev.* B **70** 104302
[17] Strout D L, Murry R L, Xu C, Eckhoff W C, Odom G K and Scuseria G E 1993 *Chem. Phys. Lett.* **214** 57
[18] Pederson M R and Quong A A 1995 *Phys. Rev. Lett.* **74** 2319
[19] Scuseria G E 1996 *Chem. Phys. Lett.* **257** 583
[20] Stephens P W, Bortel G, Faigel G, Tegze M, Jáonssy A, Pekker S, Oszlanyi G and Forró L 1994 *Nature* **370** 636
[21] Pekker S, Forró L, Mihály L and Jánossy A 1994 *Solid State Commun.* **90** 349
[22] Chopra N G, Hone J and Zettl A 1996 *Phys. Rev.* B **53** 8155
[23] Adams G B, Page J B, Sankey O F, Sinha K and Menendez J 1991 *Phys. Rev.* B **44** 4052
[24] Adams G B, Page J B, Sankey O F and O'Keeffe M 1994 *Phys. Rev.* B **50** 17471–9
[25] Menon M, Subbaswamy K R and Sawtarie M 1994 *Phys. Rev.* B **49** 13966
[26] Schober H, Tölle A, Renker B, Heid R and Gompf F 1997 *Phys. Rev.* B **56** 5937
[27] Jishi R A, Mirie R M and Dresselhaus M S 1992 *Phys. Rev.* B **45** 13685
[28] Kataura H, Maniwa Y, Abe M, Fujiwara A, Kodama T, Kikuchi K, Imahori H, Misaki Y, Suzuki S and Achiba Y 2002 *Appl. Phys.* A **74** 349
[29] Pfeiffer R, Kuzmany H, Pichler T, Kataura H, Achiba Y, Melle-Franco M and Zerbetto F 2004 *Phys. Rev.* B **69** 035404
[30] Chadli H, Rahmani A, Sbai K and Sauvajol J L 2005 *Physica* A **358** 226
[31] Bandow S, Takizawa M, Kato H, Okazaki T, Shinohara H and Iijima S 2001 *Chem. Phys. Lett.* **347** 23
[32] Bandow S, Takizawa M, Hirahara K, Yudasaka M and Iijima S 2001 *Chem. Phys. Lett.* **337** 48
[33] Allinger N L 1997 *J. Am. Chem. Soc.* **107** 8127
[34] Bendele G M, Stephens P W, Prassides K, Vavekis K, Kordatos K and Tanigaki K 1998 *Phys. Rev. Lett.* **80** 736
[35] Saito R, Takeya T, Kimura T, Dresselhaus G and Dresselhaus M S 1998 *Phys. Rev.* B **57** 4145
[36] Rahmani A, Sauvajol J-L, Rols S and Benoit C 2002 *Phys. Rev.* B **66** 125404
[37] Ulbricht H, Moos G and Hertel T 2003 *Phys. Rev. Lett.* **90** 095501
[38] Liu X, Pichler T, Knupfer M, Golden M S, Fink J, Kataura H, Achiba Y, Hirahara K and Iijima S 2002 *Phys. Rev.* B **65** 045419

[39] Kataura H, Kodama T, Kikuchi K, Hirhara K, Suenaga K, Ijima S, Suzuki S, Krätschmer W and Achiba Y 2001 *ISNM (Melville, NY: AIP)*; *AIP Conf. Proc.* **590** 165
[40] Guha S, Menéndez J, Page J B and Adams G B 1996 *Phys. Rev.* B **53** 13106
[41] Benoit C, Royer E and Poussigue G 1992 *J. Phys.: Condens. Matter* **4** 3125
[42] Renker B, Schober H, Gompf F, Heid R and Ressouche E 1996 *Phys. Rev.* B **53** R14701
[43] Lebedkin S, Gromov A, Giesa S, Gleiter R, Renker B, Rietschel H and Krätschmer W 1998 *Chem. Phys. Lett.* **285** 210
[44] Snoke D W and Cardona M 1993 *Solid State Commun.* **87** 121
[45] Rao A M, Zhou P, Wang K A, Hager G T, Holden J M, Wang Y, Lee W T, Bi X X, Eklund P C, Cornett D S, Duncan M A and Amster I J 1993 Photopolymerization of C_{60} thin films *Science* **259** 955
[46] Porezag D, Pederson M R, Frauenheim T and Köhler T 1995 *Phys. Rev.* B **52** 14963
[47] Wang Y, Holden J M, Xiang-Xin Bi and Eklund P C 1993 *Chem. Phys. Lett.* **217** 413
[48] Cambedouzou J, Rols S, Almairac R, Sauvajol J L, Kataura H and Schober H 2005 *Phys. Rev.* B **71** 041403(R)
[49] Sinha K, Menendez J, Adams G B, Page J B, Sankey O F, Lamb L D and Huffman D R 1991 *Applied Spectroscopy in Materials Science (Bellingham, WA: SPIE—The International Society for Optical Engineering)*; *Proc. SPIE* **1437** 32